Biomedical Optics EXPRESS

Intravital imaging of mouse colonic adenoma using MMP-based molecular probes with multi-channel fluorescence endoscopy

Gyungseok Oh,[1] Su Woong Yoo,[2] Yebin Jung,[3] Yeon-Mi Ryu,[4] Youngrong Park,[3] Sang-Yeob Kim,[4,5] Ki Hean Kim,[6] Sungjee Kim,[3] Seung-Jae Myung,[4,7] and Euiheon Chung[1,2,*]

[1]*School of Mechatronics, Gwangju Institute of Science and Technology, Gwangju, South Korea,*
[2]*Department of Medical System Engineering, Gwangju Institute of Science and Technology, Gwangju, South Korea,*
[3]*Department of Chemistry, Pohang University of Science and Technology, Pohang, South Korea,*
[4]*Asan Institute for Life sciences, Asan Medical Center, University of Ulsan College of Medicine, Seoul, South Korea*
[5]*Deparment of Medicine, University of Ulsan College of Medicine, Seoul, South Korea,*
[6]*Division of Integrative Biosciences and Biotechnology and Department of Mechanical Engineering, Pohang University of Science and Technology, Pohang, South Korea*
[7]*Department of Gastroenterology, Asan Medical Center,University of Ulsan College of Medicine, Seoul, South Korea*
[*]*ogong50@gist.ac.kr*

Abstract: Intravital imaging has provided molecular, cellular and anatomical insight into the study of tumor. Early detection and treatment of gastrointestinal (GI) diseases can be enhanced with specific molecular markers and endoscopic imaging modalities. We present a wide-field multi-channel fluorescence endoscope to screen GI tract for colon cancer using multiple molecular probes targeting matrix metalloproteinases (MMP) conjugated with quantum dots (QD) in AOM/DSS mouse model. MMP9 and MMP14 antibody (Ab)-QD conjugates demonstrate specific binding to colonic adenoma. The average target-to-background (T/B) ratios are 2.10 ± 0.28 and 1.78 ± 0.18 for MMP14 Ab-QD and MMP9 Ab-QD, respectively. The overlap between the two molecular probes is 67.7 ± 8.4%. The presence of false negative indicates that even more number of targeting could increase the sensitivity of overall detection given heterogeneous molecular expression in tumors. Our approach indicates potential for the screening of small or flat lesions that are precancerous.

OCIS codes: (110.0110) Imaging systems; (170.4580) Optical diagnostics for medicine; (170.3880) Medical and Biological imaging; (170.2150) Endoscopic imaging.

References and links

1. G. Oh, E. Chung, and S. H. Yun, "Optical fibers for high-resolution in vivo microendoscopic fluorescence imaging," Opt. Fiber Technol. **19**(6), 760–771 (2013).
2. J. C. van Rijn, J. B. Reitsma, J. Stoker, P. M. Bossuyt, S. J. van Deventer, and E. Dekker, "Polyp miss rate determined by tandem colonoscopy: a systematic review," Am. J. Gastroenterol. **101**(2), 343–350 (2006).
3. C. A. Munroe, P. Lee, A. Copland, K. K. Wu, T. Kaltenbach, R. M. Soetikno, and S. Friedland, "A tandem colonoscopy study of adenoma miss rates during endoscopic training: a venture into uncharted territory," Gastrointest. Endosc. **75**(3), 561–567 (2012).
4. M. W. Shahid, A. M. Buchner, M. G. Heckman, M. Krishna, M. Raimondo, T. Woodward, and M. B. Wallace, "Diagnostic accuracy of probe-based confocal laser endomicroscopy and narrow band imaging for small colorectal polyps: a feasibility study," Am. J. Gastroenterol. **107**(2), 231–239 (2012).
5. R. Kiesslich, J. Fritsch, M. Holtmann, H. H. Koehler, M. Stolte, S. Kanzler, B. Nafe, M. Jung, P. R. Galle, and M. F. Neurath, "Methylene blue-aided chromoendoscopy for the detection of intraepithelial neoplasia and colon cancer in ulcerative colitis," Gastroenterology **124**(4), 880–888 (2003).
6. J. Haringsma, G. N. Tytgat, H. Yano, H. Iishi, M. Tatsuta, T. Ogihara, H. Watanabe, N. Sato, N. Marcon, B. C. Wilson, and R. W. Cline, "Autofluorescence endoscopy: feasibility of detection of GI neoplasms unapparent to white light endoscopy with an evolving technology," Gastrointest. Endosc. **53**(6), 642–650 (2001).
7. M. C. Pierce, P. M. Vila, A. D. Polydorides, R. Richards-Kortum, and S. Anandasabapathy, "Low-cost

#207969 - $15.00 USD Received 14 Mar 2014; revised 19 Apr 2014; accepted 21 Apr 2014; published 29 Apr 2014

endomicroscopy in the esophagus and colon," Am. J. Gastroenterol. **106**(9), 1722–1724 (2011).
8. M. A. Saldua, C. A. Olsovsky, E. S. Callaway, R. S. Chapkin, and K. C. Maitland, "Imaging inflammation in mouse colon using a rapid stage-scanning confocal fluorescence microscope," J. Biomed. Opt. **17**(1), 016006 (2012).
9. P. Kim, E. Chung, H. Yamashita, K. E. Hung, A. Mizoguchi, R. Kucherlapati, D. Fukumura, R. K. Jain, and S. H. Yun, "In vivo wide-area cellular imaging by side-view endomicroscopy," Nat. Methods **7**(4), 303–305 (2010).
10. S. F. Elahi, S. J. Miller, B. Joshi, and T. D. Wang, "Targeted imaging of colorectal dysplasia in living mice with fluorescence microendoscopy," Biomed. Opt. Express **2**(4), 981–986 (2011).
11. P. B. Garcia-Allende, J. Glatz, M. Koch, J. J. Tjalma, E. Hartmans, A. G. Terwisscha van Scheltinga, P. Symvoulidis, G. M. van Dam, W. B. Nagengast, and V. Ntziachristos, "Towards clinically translatable NIR fluorescence molecular guidance for colonoscopy," Biomed. Opt. Express **5**(1), 78–92 (2014).
12. M. Goetz, "Molecular imaging in GI endoscopy," Gastrointest. Endosc. **76**(6), 1207–1209 (2012).
13. M. Li and T. D. Wang, "Targeted endoscopic imaging," Gastrointest. Endosc. Clin. N. Am. **19**(2), 283–298 (2009).
14. M. R. Emmert-Buck, M. J. Roth, Z. Zhuang, E. Campo, J. Rozhin, B. F. Sloane, L. A. Liotta, and W. G. Stetler-Stevenson, "Increased gelatinase A (MMP-2) and cathepsin B activity in invasive tumor regions of human colon cancer samples," Am. J. Pathol. **145**(6), 1285–1290 (1994).
15. J. von Burstin, S. Eser, B. Seidler, A. Meining, M. Bajbouj, J. Mages, R. Lang, A. J. Kind, A. E. Schnieke, R. M. Schmid, G. Schneider, and D. Saur, "Highly sensitive detection of early-stage pancreatic cancer by multimodal near-infrared molecular imaging in living mice," Int. J. Cancer **123**(9), 2138–2147 (2008).
16. C. Bremer, C.-H. Tung, and R. Weissleder, "In vivo molecular target assessment of matrix metalloproteinase inhibition," Nat. Med. **7**(6), 743–748 (2001).
17. J. E. Koblinski, M. Ahram, and B. F. Sloane, "Unraveling the role of proteases in cancer," Clin. Chim. Acta **291**(2), 113–135 (2000).
18. M. E. Stearns and M. Wang, "Type IV collagenase (Mr 72,000) expression in human prostate: benign and malignant tissue," Cancer Res. **53**(4), 878–883 (1993).
19. G. H. Heppner, "Tumor heterogeneity," Cancer Res. **44**(6), 2259–2265 (1984).
20. P. L. Bedard, A. R. Hansen, M. J. Ratain, and L. L. Siu, "Tumour heterogeneity in the clinic," Nature **501**(7467), 355–364 (2013).
21. J. Park, J. Nam, N. Won, H. Jin, S. Jung, S. Jung, S. H. Cho, and S. Kim, "Compact and Stable Quantum Dots with Positive, Negative, or Zwitterionic Surface: Specific Cell Interactions and Non-Specific Adsorptions by the Surface Charges," Adv. Funct. Mater. **21**(9), 1558–1566 (2011).
22. M. Mitsunaga, N. Kosaka, P. L. Choyke, M. R. Young, C. R. Dextras, S. M. Saud, N. H. Colburn, M. Sakabe, T. Nagano, D. Asanuma, Y. Urano, and H. Kobayashi, "Fluorescence endoscopic detection of murine colitis-associated colon cancer by topically applied enzymatically rapid-activatable probe," Gut **62**(8), 1179–1186 (2013).
23. G. Lanza, L. Messerini, R. Gafà, M. Risio Gruppo Italiano Patologi Apparato Digerente (GIPAD)Società Italiana di Anatomia Patologica e Citopatologia Diagnostica/International Academy of Pathology, Italian division (SIAPEC/IAP), "Colorectal tumors: the histology report," Dig. Liver Dis. **43**(Suppl 4), S344–S355 (2011).
24. G. P. Boivin, K. Washington, K. Yang, J. M. Ward, T. P. Pretlow, R. Russell, D. G. Besselsen, V. L. Godfrey, T. Doetschman, W. F. Dove, H. C. Pitot, R. B. Halberg, S. H. Itzkowitz, J. Groden, and R. J. Coffey, "Pathology of mouse models of intestinal cancer: consensus report and recommendations," Gastroenterology **124**(3), 762–777 (2003).
25. R. Upadhyay, R. A. Sheth, R. Weissleder, and U. Mahmood, "Quantitative real-time catheter-based fluorescence molecular imaging in mice," Radiology **245**(2), 523–531 (2007).
26. M. Gerlinger, A. J. Rowan, S. Horswell, J. Larkin, D. Endesfelder, E. Gronroos, P. Martinez, N. Matthews, A. Stewart, P. Tarpey, I. Varela, B. Phillimore, S. Begum, N. Q. McDonald, A. Butler, D. Jones, K. Raine, C. Latimer, C. R. Santos, M. Nohadani, A. C. Eklund, B. Spencer-Dene, G. Clark, L. Pickering, G. Stamp, M. Gore, Z. Szallasi, J. Downward, P. A. Futreal, and C. Swanton, "Intratumor heterogeneity and branched evolution revealed by multiregion sequencing," N. Engl. J. Med. **366**(10), 883–892 (2012).
27. M. D. Baugh, M. J. Perry, A. P. Hollander, D. R. Davies, S. S. Cross, A. J. Lobo, C. J. Taylor, and G. S. Evans, "Matrix metalloproteinase levels are elevated in inflammatory bowel disease," Gastroenterology **117**(4), 814–822 (1999).
28. A. K. Steingräber, S. Schelhaas, A. Faust, A. H. Jacobs, M. Schäfers, and T. Goerge, "Molecular imaging reveals time course of matrix metalloproteinase activity in acute cutaneous vasculitis in vivo," Exp. Dermatol. **22**(11), 730–735 (2013).
29. M. Oshima, J. E. Dinchuk, S. L. Kargman, H. Oshima, B. Hancock, E. Kwong, J. M. Trzaskos, J. F. Evans, and M. M. Taketo, "Suppression of Intestinal Polyposis in *Apc* $^{\Delta 716}$ Knockout Mice By Inhibition Of Cyclooxygenase 2 (COX-2)," Cell **87**(5), 803–809 (1996).
30. A. K. Steingräber, S. Schelhaas, A. Faust, A. H. Jacobs, M. Schäfers, and T. Goerge, "Molecular imaging reveals time course of matrix metalloproteinase activity in acute cutaneous vasculitis in vivo," Exp. Dermatol. **22**(11), 730–735 (2013).
31. S. M. Yoon, S.-J. Myung, B. D. Ye, I.-W. Kim, N. G. Lee, Y. M. Ryu, K. Park, K. Kim, I. C. Kwon, Y. S. Park, C. S. Park, D. H. Moon, H. Kim, M. Y. Do, J. S. Byeon, S. K. Yang, and J. H. Kim, "Near-infrared fluorescence

#207969 - $15.00 USD Received 14 Mar 2014; revised 19 Apr 2014; accepted 21 Apr 2014; published 29 Apr 2014

imaging using a protease-specific probe for the detection of colon tumors," Gut Liver **4**(4), 488–497 (2010).
32. R. Atreya and M. Goetz, "Molecular imaging in gastroenterology," Nat Rev. Gastroenterol. Hepatol. **10**(12), 704–712 (2013).
33. M. Mitsunaga, N. Kosaka, P. L. Choyke, M. R. Young, C. R. Dextras, S. M. Saud, N. H. Colburn, M. Sakabe, T. Nagano, D. Asanuma, Y. Urano, and H. Kobayashi, "Fluorescence endoscopic detection of murine colitis-associated colon cancer by topically applied enzymatically rapid-activatable probe," Gut **62**(8), 1179–1186 (2013).
34. M. G. Tutton, M. L. George, S. A. Eccles, S. Burton, R. I. Swift, and A. M. Abulafi, "Use of plasma MMP-2 and MMP-9 levels as a surrogate for tumour expression in colorectal cancer patients," Int. J. Cancer **107**(4), 541–550 (2003).
35. X. Wu, H. Liu, J. Liu, K. N. Haley, J. A. Treadway, J. P. Larson, N. Ge, F. Peale, and M. P. Bruchez, "Immunofluorescent labeling of cancer marker Her2 and other cellular targets with semiconductor quantum dots," Nat. Biotechnol. **21**(1), 41–46 (2002).
36. Z. Popović, W. Liu, V. P. Chauhan, J. Lee, C. Wong, A. B. Greytak, N. Insin, D. G. Nocera, D. Fukumura, R. K. Jain, and M. G. Bawendi, "A nanoparticle size series for in vivo fluorescence imaging," Angew. Chem. Int. Ed. Engl. **49**(46), 8649–8652 (2010).
37. V. P. Chauhan, T. Stylianopoulos, J. D. Martin, Z. Popović, O. Chen, W. S. Kamoun, M. G. Bawendi, D. Fukumura, and R. K. Jain, "Normalization of tumour blood vessels improves the delivery of nanomedicines in a size-dependent manner," Nat. Nanotechnol. **7**(6), 383–388 (2012).
38. Y. Park, Y.-M. Ryu, Y. Jung, T. Wang, Y. Baek, Y. Yoon, M.B. Sang, J. Park, S. Hwang, J. Kim, S.-Y. Kim, E. Chung, K.H. Kim, S. Kim, and S.-J. Myung, *Raid and Multiplexed Quantum Dot Conjugate Spraying Probes for Colonoscopic Cancer Diagonosis.*
39. Y. Urano, M. Sakabe, N. Kosaka, M. Ogawa, M. Mitsunaga, D. Asanuma, M. Kamiya, M.R. Young, T. Nagano, and P.L. Choyke, *Rapid cancer detection by topically spraying a γ-glutamyltranspeptidase–activated fluorescent probe.* Sci Transl Med, 2011. **3**(110): p. 110ra119–110ra119.
40. Y. Li, Z. Li, X. Wang, F. Liu, Y. Cheng, B. Zhang, and D. Shi, "In vivo cancer targeting and imaging-guided surgery with near infrared-emitting quantum dot bioconjugates," Theranostics **2**(8), 769–776 (2012).
41. L. Barault, N. Veyrie, V. Jooste, D. Lecorre, C. Chapusot, J. M. Ferraz, A. Lièvre, M. Cortet, A. M. Bouvier, P. Rat, P. Roignot, J. Faivre, P. Laurent-Puig, and F. Piard, "Mutations in the RAS-MAPK, PI(3)K (phosphatidylinositol-3-OH kinase) signaling network correlate with poor survival in a population-based series of colon cancers," Int. J. Cancer **122**(10), 2255–2259 (2008).
42. X. Cui, Y. Jin, D. Poudyal, A. A. Chumanevich, T. Davis, A. Windust, A. Hofseth, W. Wu, J. Habiger, E. Pena, P. Wood, M. Nagarkatti, P. S. Nagarkatti, and L. Hofseth, "Mechanistic insight into the ability of American ginseng to suppress colon cancer associated with colitis," Carcinogenesis **31**(10), 1734–1741 (2010).
43. R. Xie, U. Kolb, J. Li, T. Basché, and A. Mews, "Synthesis and characterization of highly luminescent CdSe-core CdS/Zn0.5Cd0.5S/ZnS multishell nanocrystals," J. Am. Chem. Soc. **127**(20), 7480–7488 (2005).

1. Introduction

Early detection and the removal of precancerous lesions have been shown to reduce mortality rate associated with colon cancer and this could be aided by specific markers and endoscopic imaging modalities. An endoscope can transmit light deep into the body through optical fibers and visualize lesions that are typically inaccessible by other means [1]. However, it has several limitations in detecting small lesions or identifying microscopic pathological features. For example, conventional colonoscopic diagnosis with white light can miss up to 20% of adenomas [2, 3]. Routine colonoscopy procedures cannot provide histopathologic information by itself, and sometimes requires unnecessary biopsy or removal of suspected lesions for diagnosis, often requiring patients to revisit for additional biopsies or examinations. Thus, several methods to improve its accuracy to identify dysplasia or cancer have been proposed including narrow-band imaging, autofluorescence imaging and chromoendsocopy [4–6]. High-resolution endoscopy with preclinical animal models has revealed microscopic details in disease progression [7–9]. However, these modalities have fluctuating results for detecting colon cancer due to limited molecular specificity.

Recently, molecular imaging has emerged in gastroenterology by use of fluorescently labeled probes to specifically highlight neoplastic lesions on the basis of their molecular signatures [10–12]. Neoplastic lesions often overexpress certain receptors or enzymes in transformed mucosa. These contrasts between normal and abnormal tissue provide an effective method of detection with imaging techniques. Proteases are potential candidates of molecular targets as proteolytic enzymes play an important role in cell proliferation, invasion, angiogenesis and metastasis. These enzymes provide important means for the detection and

#207969 - $15.00 USD Received 14 Mar 2014; revised 19 Apr 2014; accepted 21 Apr 2014; published 29 Apr 2014

diagnosis of cancer in the digestive tract, for example, colon cancer [13, 14]. Matrix metalloproteinase (MMP) enable malignant cells to breach basement membranes and subsequently invade neighboring tissues. Several MMPs are expressed in cancers at much higher levels than in normal tissue. The extent of expression is known to be related to tumor stage [15–18].

With specific molecular targets labeled with distinct fluorescent molecules such as quantum dots, wide-field fluorescence endoscope enables rapid imaging of large mucosa in GI tract to screen potentially cancerous lesions. Together with white-light imaging, fluorescence endoscopic imaging can be realized with emission filters and excitation light sources. This approach can provide a red flag imaging technique for the detection of suspicious lesions. In preclinical study, this imaging system could be used for characterization and visualization of molecular probes that are supposed to bind to specific targets associated with tumor. As molecular expression of tumors is known to be heterogeneous, multiple molecular targeting strategies could increase the detection specificity of tumor screening [19, 20].

Here we show the endoscopic imaging of colonic adenoma in a colon cancer mouse model with multiple MMP antibody–quantum dot (MMP Ab-QD) conjugates with a home-modified wide-field multi-channel fluorescence endoscope.

2. Materials and methods

2.1 AOM/DSS colorectal cancer model

4-week-old female BALB/c mice (DBL, Eumseong, South Korea) were used for this study. After acclimatization for seven days with basal diet and standard water feeding, single intraperitoneal (i.p.) injection of AOM (10 mg/kg body weight; Sigma–Aldrich, MO, USA) was done for all mice. One week later, drinking water containing 2% DSS (MP biomedicals, Illkirch, France) was administered for 7 days. Then the drinking water switches back to standard drinking water for 2 weeks. This administration method of DSS in the drinking water was repeated. All mice were weighed twice per week. To check tumor formation in the colonic wall, colonoscopic examination was performed. All animal experiments were performed with protocols approved by the Institutional Animal Care and Use Committee (IACUC) of the Gwangju Institute of Science and Technology.

2.2 Preparation of targeted fluorescence molecular probes

MMP9 and MMP14 Ab were conjugated with red and yellow light emitting QD (MMP9 Ab-Red QD and MMP14 Ab-Yellow QD, respectively). Two different color emitting CdSe/CdS/ZnS(Core/Shell/Shell) QDs were synthesized using procedures previously published (See Appendix Section) [21]. The absorption and fluorescence profiles of probes are shown in Fig. 1, where the emission peaks can be found at 585 and 630 nm, respectively. The QD surface was co-decorated with a zwitterionic ligand and a ligand bearing carboxylic acid. The carboxylic acids were used for conjugation with MMP9 Ab and MMP14 Ab [21].

#207969 - $15.00 USD Received 14 Mar 2014; revised 19 Apr 2014; accepted 21 Apr 2014; published 29 Apr 2014

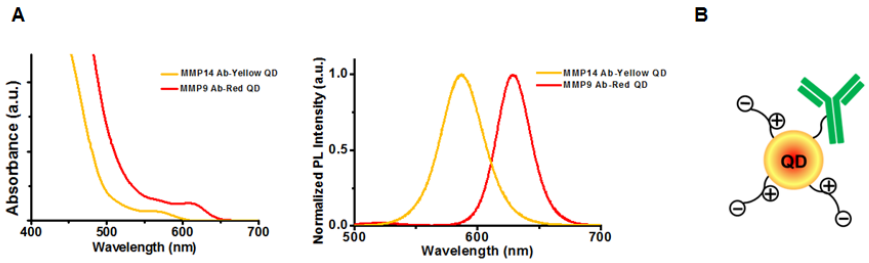

Fig. 1. Characteristics of matrix metalloproteinase (MMP) antibody (Ab) -quantum dot (QD) probes. (A) Absorbance and photoluminescence (PL) spectra of MMP9 Ab-Red QD and MMP14 Ab-Yellow QD. (B) Scheme for Ab-QD conjugation.

2.3 Multi-channel fluorescence and white light imaging endoscope setup

To image molecular fluorescence from mouse colonic mucosa, we constructed multi-channel fluorescence endoscopic system using a commercial endoscope probe (HOPKINS II Telescope 27301AA, Karl Storz, Tuttlingen, Germany) by adding detection and excitation light paths (Fig. 2). The detection part composes of endoscopic probe, emission filter wheel with various filters, an achromatic lens (f = 50 mm, Thorlabs, NJ, USA), sensitive color charge coupled device (CCD) camera (QIClick, QImaging, Surrey, BC, Canada), an inflating pump for mildly inflating the colon during imaging and a white light source (LS-100W, Light Solution, Cheonan, Korea). The excitation light is generated from a laser source with wavelength of473nm (Shaghai Dream Lasers Technology, SDL-473-300T,Shanghai, China) that excites corresponding fluorescent probes after coupling into two coherent fiber bundles (FIGH-10-500N, Fujikura, Tokyo, Japan).

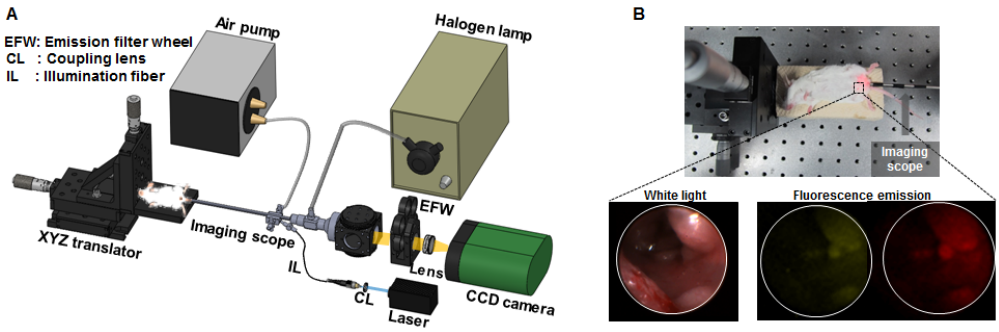

Fig. 2. Multi-channel fluorescence endoscopy system. (A) Scheme of the system. Excitation laser beams (473 nm) are delivered into illumination fibers. Reflected- and emitted light from the colonic tissues is detected by endoscope. Collected lights are focused on charge coupled device (CCD) camera with additional fluorescence light filtering through proper emission filters. (B) Photograph of system and close-up view of imaging scope.

Endoscopic images were obtained via the imaging scope with white light and emitted fluorescence light after the excitation light exits the distal end of the fiber bundles to illuminated specimen. The reflected light by the white light source was displayed to form a white light image onto the color CCD camera and fluorescence passes through emission filters (FF02-628/40-25 and FF01-579/34-25, Semrock, NY, USA) prior to detection with another CCD camera. The imaging scope and the achromatic lens combination form a magnified image on the sensor of the CCD camera, which is visualized on the computer monitor with commercial software (QCapture, QImaging, Surrey, BC, Canada). The exposure time of the CCD camera was adjusted from 100 μs to 1sdepending on the sample brightness. The system achieves the lateral resolution of 44 μm and field of view of 7.5 mm at a working

#207969 - $15.00 USD Received 14 Mar 2014; revised 19 Apr 2014; accepted 21 Apr 2014; published 29 Apr 2014

distance of 5 mm using USAF 1951 resolution target (R3L2S1P, Thorlabs, NJ, USA). We performed a controlled experiment *in vitro* to determine the detection limit of our fluorescence endoscope by imaging Red QD samples with known concentrations of 1.01×10^{11}, 2.00×10^{10} and 4.00×10^{9} (QDs/mm^2) as well as the background with typical operating condition (exposure time of 500 ms). We obtained the detection of limit of our fluorescence endoscope as 8.60×10^{9} (QDs/mm^2) based on the Rose criterion of SNR of five. However determination of the detection limit *in vivo* is non-trivial as the actual concentration of the molecular probes at the tumor lesion depends on each tumor and varies over time even with controlled amount of injection.

2.4 In vivo molecular fluorescence imaging of colonic tumors

For evaluation of each molecular probe, four mice were used for MMP9 Ab-Red QD and three mice were used for MMP14 Ab-Yellow QD. Prior to imaging inside mouse colon, the colon was washed with phosphate buffered saline (PBS) to remove debris. The endoscopic imaging with white light was performed to identify the presence of adenomas. Animals bearing tumors were injected intravenously via tail vein with each molecular probe (concentration: 100 nM, volume: 100 μL). The mice were gas anesthetized with isoflurane. Many molecularly targeting imaging relies on labeling target-specific molecules after intravenous (i.v.) injection when enough probes bind to their targets. The method has been particularly useful for imaging receptors and cell-surface-expressed molecular targets. After i.v. injection of MMP Ab-QD conjugates, we measured fluorescence signal from tumor of AOM/DSS mouse model at designated time points using 579/34 nm and 628/40 nm emission filter with 473 nm excitation and compared the signal value and target-to-background (T/B) ratio. Typical imaging area was located in 0.5 cm to 3.0 cm depth from the anus of the mouse. By 12 hours after i.v. injection of MMP14 Ab-Yellow QD, the fluorescence intensity was increased. However, the peak of fluorescence intensity was increased by 24 hours after i.v. injection of MMP9 Ab-Red QD. Although the peak times were different, each T/B ratio at 12hours after injection of the probes was larger than at 24 hours (Fig. 8).

In addition, we concomitantly injected two molecular probes intravenously with the same concentration (100 nM) and volume (100 μL) and imaged 12 hours after injection. In order to determine the fluorescence T/B ratio, snap shot images were used for quantifying fluorescence intensities. All fluorescence images were analyzed with the Image J software (National Institutes of Health, USA). Circular ROIs were place in the tumor (S_t) and in adjacent normal mucosa (S_n). All ROI intensities were recorded in pixel intensity values between 0 and 255. After obtaining mean signal intensities, the T/B ratio was determined as S_t/S_n [22]. Data are presented as means ± standard deviation of the mean, and each signal intensity value represents either tumor or normal mucosa signal intensity subtracted by background signal intensity (intrinsic camera noise). The significance of differences between signal intensity values was determined by using Mann-Whitney U test. $P<0.05$ was considered to indicate significant difference. Analysis was performed with the statistical software package for social science (SPSS, version 19.0.0; Chicago, IL, USA).

2.5 Ex vivo colon tissue fluorescence imaging by molecular probes

Two and three AOM/DSS mice model (age over 12 weeks old) were used for *ex vivo* fluorescence imaging with control IgG-QD and MMP Ab-QDs, respectively. For ex-vivo mouse colon tissue imaging, tumor-bearing mice were sacrificed and the colons were longitudinally excised. The excised colon tissues were incubated in 100 nM MMP9-Ab Red QD and MMP14-Ab Yellow QD (with IgG- yellow QD, IgG- red QD, respectively) for 30 min at the same time. These tissues were subsequently rinsed three times with 1X PBS. The fluorescence signal, expressed at the colon tissue (Fig. 6F-6H), was obtained using the IVIS spectrum system (Perkin Elmer, MA, USA). Images were acquired with excitation at 430 nm and emission at 500-800 nm using auto acquisition, a binning factor of 8 and field of view of

#207969 - $15.00 USD Received 14 Mar 2014; revised 19 Apr 2014; accepted 21 Apr 2014; published 29 Apr 2014

13.4 cm. Final fluorescence imaging was obtained with spectral unmixing using the Living Image® 4.3.1 software (Perkin Elmer, MA, USA) and was quantified radiant efficiency.

2.6 Histologic analysis of excised colon tumor

Twenty-four hours after molecular probes were injected, mice were sacrificed and the colons were surgically excised. The colon tissues were examined *ex vivo* using optical imaging system followed by hematoxylin and eosin (H&E) staining. For histopathological evaluation, normal and tumoral lesions were excised, fixed for 24 hours in 4% (w/v) paraformaldehyde prior to H&E stain. Each specimen was examined by an experienced pathologist using standard published criteria [23, 24].

2.7 Quantitative fluorescence image correction based on reflection image

We analyzed experimental images based on previous quantitative fluorescence molecular imaging [25]. As the integration time affect the amount of signal, we kept the same integration time for quantitative comparisons between experimental groups that maximizes the use of dynamic range of our CCD detector. Corrected fluorescence signal intensity was calculated by dividing the fluorescence image by a sequentially acquired white light image on a pixel-by-pixel basis. Prior to analysis, all pixels outside the circular endoscopic field of view (FOV) were set to zero on the corrected image. Afterwards we set the threshold value as the average of maximum value and minimum value of the images. We compared several threshold settings such as 25%, 50%, and 75% of the min-max value of the fluorescence image, and found 50% threshold gave better correlation with tumor boundary based on white-light endoscopic imaging. Although this simple approach works reasonable in our AOM/DSS tumor model and QD conjugated molecular probes, we may need to use more sophisticated threshold techniques for other situations such as depressed tumor and serrated tumor.

3. Results

3.1 Intravital examination of MMP-bound colon tumors with wide-field fluorescence endoscope

The specific binding activity of the MMP targeted probe for colonic adenomas was assessed *in vivo* in 2 groups of mice. First, we randomly assigned three mice per group from those which developed grossly visible tumors by performing white light endoscopy. Twelve hours after MMP targeted probes were injected intravenously, fluorescence imaging was performed for two groups: (1) MMP14 Ab-Yellow QD (six tumors in 3 animals) and (2) MMP9 Ab-Red QD (seven tumors in 4 animals). The images from white light endoscopy of a representative adenoma are shown in Fig. 3(A) and 3(D). Specific binding of each MMP targeted probe to corresponding colonic tumor is demonstrated by comparing the fluorescence images collected with the white light endoscopy (Fig. 3(B) and Fig. 3(E)). In Fig. 3(B), MMP14-Yellow QD demonstrated obvious contrast that enabled detection of flat lesions compared with white light image in Fig. 3(A). From histological inspection, the presence of adenoma was confirmed (Fig. 3(C)). In addition MMP9 Ab-Red QD probe was used to detect suspicious tumor lesion in different animal. The T/B ratio arising from fluorescent lesions was significantly higher than unity compared with surrounding non-fluorescent lesions. The fluorescence images of colonic adenoma collected with MMP14 Ab-Yellow QD and MMP9 Ab-Red QD shows increased signal over adjacent surface with a T/B ratio of 2.10 ± 0.28 (average ± standard deviation) and 1.78 ± 0.18, respectively. H&E of the adenoma is shown in Fig. 3(C) and 3(F).

#207969 - $15.00 USD Received 14 Mar 2014; revised 19 Apr 2014; accepted 21 Apr 2014; published 29 Apr 2014

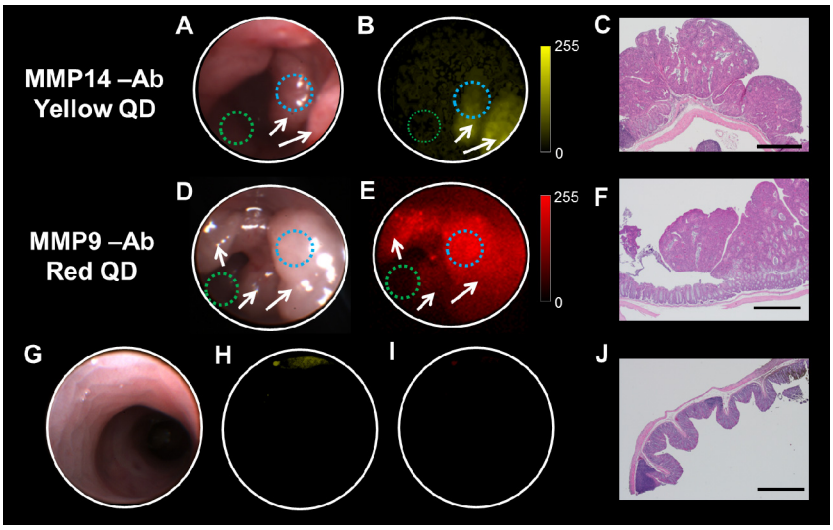

Fig. 3. Specific binding of molecular probe *in vivo*. Tumor lesions (white arrows) are showed in white light images (A, D). These lesions are well-localized on fluorescence images by MMP14 Ab-Yellow QD (B, white arrow) and MMP9-AbRed QD (E, white arrows). Blue-and green-dotted circles on images are representative region of tumor and normal tissues, respectively. Hematoxylin and eosin (H&E) staining (C, F) showed adenomatous features including distorted crypt architecture, and normal appearing adjacent colonic mucosa. Colonic adenomas were localized on fluorescence images with two molecular probes. However, in mouse which has no tumoral lesion (G), there is no significant accumulation of MMP14 Ab-Yellow QD (H) and MMP9 Ab-Red QD (I). H&E staining from normal mouse (J) shows normal crypt. Scale bar: 200 μm.

In Fig. 3(G)-3(J),endoscopic imaging with (H) MMP14-Yellow QD and (I) MMP9-Red QD probes to normal colonic mucosa of control animal gave little signal with matching emission filters as the molecular probes have negligible binding to normal colonic mucosa.

3.2 Early detection of flat colonic tumor with MMP14-based molecular probe

Use of MMP14 Ab-Yellow QD achieved specific contrast enhancement that enabled detection of suspicious flat lesions that could have been missed with white light endoscopy. A suspicious region was identified with white light imaging (Fig. 4(A)) and subsequent fluorescence imaging based on MMP14 Ab-Yellow QD probe revealed the presence of flat tumor (In Fig. 4(B), white arrow) that was confirmed later as adenoma from histological inspection(Fig. 4(C)).

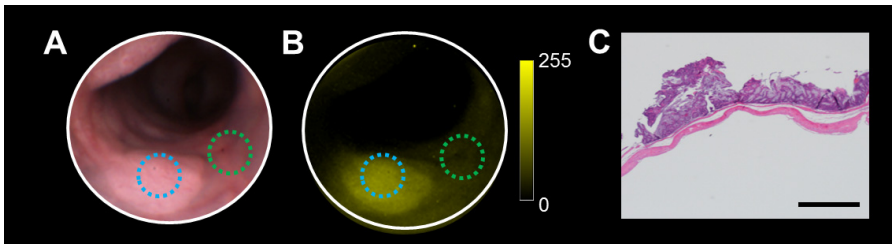

Fig. 4. Early detection of colonic tumor *in vivo*. (A) White light image of early tumoral lesion of colon (white arrow). (B) MMP14 Ab-Yellow QD is accumulated in tumoral lesion (white arrow) molecular probe. Blue-and green-dotted circles on images are representative region of tumor and normal tissues, respectively. (C) Histologic evaluation of this lesion shows features of high-grades of adenoma. Scale bar: 200 μm.

#207969 - $15.00 USD Received 14 Mar 2014; revised 19 Apr 2014; accepted 21 Apr 2014; published 29 Apr 2014

3.3 Multi-channel tumor targeted fluorescence images from multiple molecular probes

To increase the sensitivity of detection for screening purpose, the simultaneous examination of multiple molecular targets with distinct fluorescent QD labels were tried. Twelve hours prior to endoscopic imaging we sequentially injected MMP14 Ab-Yellow QD and MMP9 Ab-Red QD probes intravenously both with the concentration of 100 nM and the volume of 100 μL. In a representative white light image (Fig. 5(A)), three suspicious colonic adenomas from a representative AOM/DSS treated animal is indicated with white arrows. The lesions with different sizes and shapes were identifiable in both channels. Using two separate fluorescent emission channels, each binding patterns to colonic tumors can be displayed (Fig. 5(F) and 5(G)), and the overlapping area was shown as a merged image in Fig. 5(H) based on the fluorescence correction method described in the *Materials and Methods*.

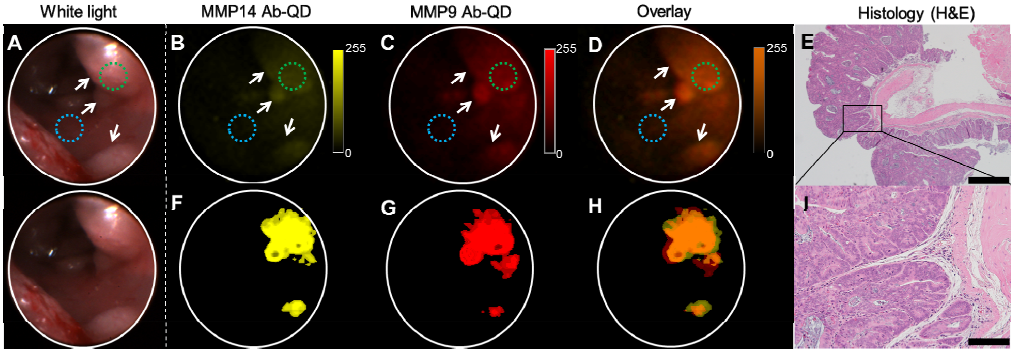

Fig. 5. Multi-color fluorescence imaging by molecular probes. White light image (A) showed suspicious tumor lesion (white arrows). (B) MMP14 Ab-Yellow QD, (C) MMP9 Ab-Red QD and (D) Merged image (B) and (C) images showed similar accumulation pattern to tumor lesion. Blue-and green-dotted circles on images are representative region of tumor and normal tissues, respectively. (E) Histologic evaluation of this lesion shows features of high-grades of adenomas, magnification 4x and (I) enlarged image of (E), magnification 20x. (F-H) Quantitative fluorescence image. (F) MMP14-Yellow QD and (G) MMP9-Red QD. (H) Overlaid image of (F) and (G). Scale bar (E) 200 μm and (I) 50μm.

There was a substantial overlap between two distinguished areas highlighted with each molecular probe used (overlap ratio = 83.8 ± 5.4% (MMP14 Ab-Yellow QD), 77.8 ± 6.7% (MMP9 Ab-Red QD) and 67.7 ± 8.4% (both MMPs) with n = 7 lesions in three animals). After fixation, the lesion was confirmed as high-grade adenoma from the inspection of H&E staining. These results suggest that both MMP-based molecular probes bind to similar locations within the AOM/DSS colon tumors.

While the combination of MMP9 and MMP14-based probes effectively showed the detection of common tumor lesion, the two molecular targeting probes might not be sufficient. As an example, we also found lesions where two clearly identifiable tumors with white light endoscopy did not give signals in both molecular channels. While both MMP-QD probes were overexpressed in one tumor (white arrow), no signal was detected in a neighboring tumor (red arrow) (Fig. 6).

#207969 - $15.00 USD Received 14 Mar 2014; revised 19 Apr 2014; accepted 21 Apr 2014; published 29 Apr 2014

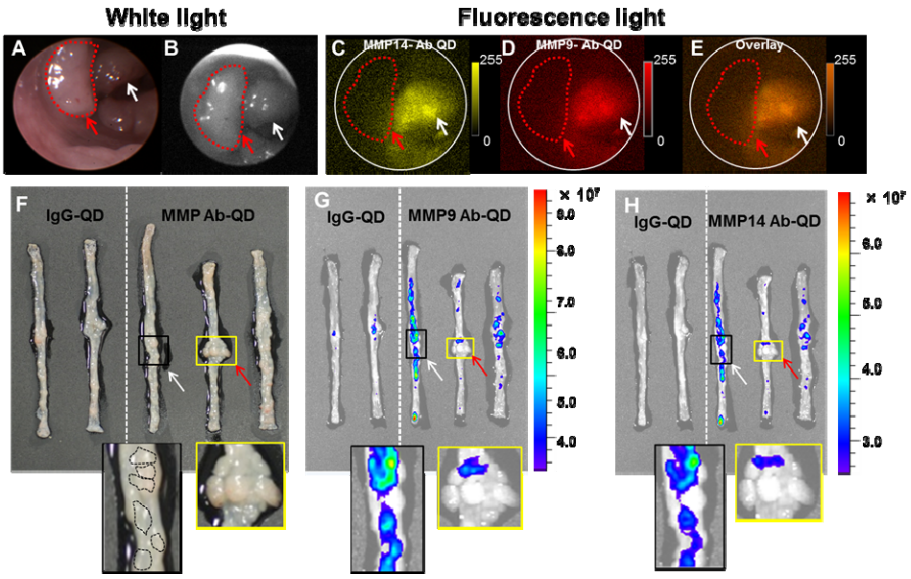

Fig. 6. Tissue-selective binding of molecular probes. White light images from colonic adenomas (A, B) showed several tumoral lesions. Sequential i.v. injection of MMP14-Yellow QD (C) and MMP9 Ab-Red QD (D) results in similar patterns of binding to colonic dysplasia. Overlaid image (E) results shows colocalization of two probes. Some tumor is not bounded with MMP9 and MMP14 molecular probes (red dotted line). *Ex vivo* colon tissue imaging with (F) White light, (G) MMP14 Ab-Red QD and (H) MMP14 Ab-Yellow QD using IVIS Spectrum. Dotted lines in the white light image (inset of F) indicate tumors.

We prepared another set of AOM/DSS-treated mice. The excised colons were imaged by IVIS imaging system after stained by control IgG-QD conjugate (n = 2) and MMP Ab-QD (MMP14 Ab-yellow QD and MMP9 Ab-Red QD, n = 3). While control IgG-QD probe showed minimum non-specific signal among tumor site, MMP9 and MMP14 Ab-QD probes showed noticeable signals throughout tumor sites. As the *in vivo* observation showed in Fig. 5, some relatively large tumors did not show signal with molecular fluorescence channels as exemplified in the yellow inset of Fig. 6(G) and 6(H). These tumors may have less availability for the molecular probes to infiltrate (indicated by red arrow in Fig. 6(G) and 6(H)). MMP-based molecular probes were bound to similar suspicious tumor lesion both *in vivo* and *ex vivo* image.

4. Discussions and conclusion

We present *in vivo* wide-field multi-channel fluorescence endoscopic imaging adapted from a commercial rodent colonoscope with AOM/DSS mouse colon cancer model. The system is designed with a rigid endoscope coupled to a laser source and filter wheel, and consolidated into a single camera that provides both white light and molecular information. The general color CCD has limitation based on Bayer filter which would affect the ability of the CCD to perform accurate and efficient fluorescent imaging in the visible band. To reduce this limitation, we used scientific grade color CCD camera for detecting fluorescence signal.

For molecular targeting, we synthesized multiple MMP antibody-QD probes for endoscopic observation towards screening purpose. Among MMPs, MMP9 and MMP14 are proteloytic enzymes and are known to play a significant role in cancer transformation of mucosa in the gastrointestinal tract. While various mouse models have been used for study of colon cancer, we used azoxymethane (AOM)/dextran sulfate sodium (DSS) model that has gained popularity due to its reproducibility to form sporadic tumors. MMP9 and MMP14 antibody-QD conjugates were used both individually and simultaneously to screen

#207969 - $15.00 USD Received 14 Mar 2014; revised 19 Apr 2014; accepted 21 Apr 2014; published 29 Apr 2014

precancerous lesions over large mucosal surface area. Based on pharmacokinetic data with multiple MMP Ab-QD probes, we identified 12 hours after i.v injection to maximize the accumulation of the probes in tumor region while the unbound or nonspecific probes were cleared. The non-specific binding of QD probes are supposed to be minimal as they were designed with anti-fouling zwitterionic QD surface coating. The average T/B ratios of MMP14 Ab-QD and MMP9 Ab-QD (Fig. 7(B)) that were bound to colonic adenomas identified from endoscopic imaging were not significantly different.

Tumor-specific fluorescence signal by two molecular probes can be found at suspected lesions and these molecular probes are expressed similarly in both tumor lesions (Fig. 7). However, these (MMP9 and MMP14) may not be enough to detect all. With MMP9 Ab-Red QD probe, twelve out of fourteen tumors were detectable with seven AOM/DSS mice while eleven out of thirteen tumors were detectable with six AOM/DSS mice with MMP14 Ab-Yellow QD. Potential reasons could include the dissimilar delivery of molecular probes into one tumor that might not be perfused well or fundamental absence of corresponding molecular targets in the tumor. Either way could be explained as tumor heterogeneity [19, 20, 26]. Another potential reason for this phenomenon might be linked to inflammatory process as we used colitis-induced colon cancer mouse model [27]. In the later stage inflammatory process, the MMP expression rate of MMP was lower [28]. In addition, another inflammatory biomarker, COX-2, also showed similar tendency [29]. Therefore, MMP expressions of tumors could be heterogeneous with different inflammatory stage [30]. Treatment of mice with AOM and DSS rapidly and effectively models human colitis-associated cancer. While this model is highly popular in the study of colon tumor development in the setting of inflammation, limitations still exist. Like most other colon cancer models, AOM/DSS tumors rarely progressed to produce metastasis. Currently we are developing other colon cancer models with metastatic potential to see if our finding with MMP-based detection also applies in similar fashion. Yoon *et al.* used MMP-activatable probe in *ex vivo* colon tissue with AOM/DSS mouse model [31]. In their study, the sensitivity was 82% that is comparable to our sensitivity of 85.7% (MMP9) and 84.6% (MMP14). Their probe showed relatively higher T/B ratio of 5.70 ± 2.30 than our T/B ratio of 1.78 ± 0.18 (MMP9) and 2.10 ± 0.28 (MMP14) as their activatable probe could minimize background signal though there exists potential toxicity issue [32]. Lately, a topically applied enzymatically activatable probe targeting cancer associated enzyme showed rapid detection and high target-to-background in murine colon cancer model [33].

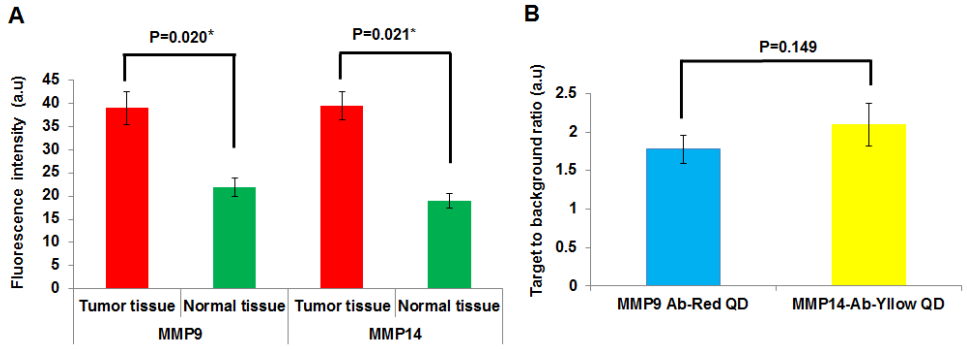

Fig. 7. Quantitative analysis of tumor specific molecular probes from intravital endoscopic imaging. (A) Comparison of fluorescence intensity between tumor and normal mucosa in 3 mice. Fluorescence signals at tumor is higher than normal tissue by MMP9 and MMP14 molecular probes (n = 3). (B) Comparison of T/B ratios of two molecular probes.

The use of QDs have several unique advantages allowing multiple colors in visible spectrum range and can be extended to more number of channels in the near-infrared window with only single excitation source due to relatively narrow and symmetric emission spectrum.

#207969 - $15.00 USD Received 14 Mar 2014; revised 19 Apr 2014; accepted 21 Apr 2014; published 29 Apr 2014

The antibody-based QD conjugates allow high specificity and affinity to molecular targets. Previous literature showed overexpression of MMP in human tumor lesion by immunohistochemistry staining with organic dyes [34]. In addition, QD conjugate with antibody was shown to be superior in terms of brightness and photostability over organic dye conjugate with antibody [35]. As the extent of probe distribution decreases with bigger size and increases steric hindrances, large nanoparticles will have more difficulty to enter into tumors. According to previous reports that probe the size-dependent QD distribution in solid tumors, our MMP Ab-QD conjugate with diameter of 22 nm is likely to reach between 60 to 80 μm from each blood vessel at 60 min post-injection [36, 37].

However, the potential toxicity issue of QDs could limit this approach only for preclinical study. In mitochondrial activity assay using human colorectal adenoma and human normal colon cell lines, our QDs did not show noticeable cytotoxicity up to a concentration of 600 nM for 24 hours [38]. In addition, there are several challenges yet to be resolved for clinical application of current approach. The application of molecular probe via i.v. injection require relatively high dose increasing costs and takes more time for optimal accumulation within the tumor tissue compared with spraying method or enzyme-activated probes although these have their own issues including penetration depth and washing-step dependency [38, 39]. Our study demonstrated two targeting molecules which may be affected by same tumorigenesis pathway. Therefore, additional targeted molecular probes would be necessary to reduce false-negatives and increase the sensitivity of screening. Due to the enhanced permeability and retention (EPR) effect, non-specific signal exists in the tumor. However, specific uptake would be bigger than non-specific uptake based on published study showing the active targeting of tumor-specific QD bioconjugates showed higher signal intensity (5 times) than the passive targeting of non-targeted QD [40].

Choosing other protein targets with orthogonal tumorigenesis pathways may increase the sensitivity for tumor detection. Therefore, we planned to use multiple promising targeting agents. Potential molecular targets for colon cancer are epidermal growth factor receptor (EGFR), human epidermal growth factor receptor 2 (HER2), and phosphoinositide 3-Kinase (PI3K) [13, 41, 42]. While two channels were demonstrated in this study, multiple molecular probes conjugated with distinct QDs and the home-modified endoscope with white light and multi-channel fluorescence offers detection of small or flat tumors and monitoring of tumor progression in real time with full fluorescence capabilities in preclinical study colon cancer.

Appendix A: synthesis of quantum dots and antibody-quantum dots conjugates

CdSe/CdS/ZnS (Core/Shell/Shell) QDs with the emission peak at 585 and 630 nm were prepared by typical synthesis method [43]. QD's surface was co-decorated by zwitterions and carboxylates by surface ligand exchange procedures previously reported elsewhere [21]. 1-ethyl-3-(3-dimethylaminopropyl)carbodiimide (EDC, 100eq to QDs) and N-hydroxysulfo-succinimide(S-NHS, 200eq to QDs) were added to mixed-ligand exchanged QDs with zwitterionic ligand and carboxylate ligand (The ratio of zwitterionic ligand to carboxylate ligand was 1:1) in 50 mM MES buffer. After 10 minute vortexing, the excess EDC and S-NHS were dialyzed using 2-(N-morpholino)ethanesulfonic acid (MES) buffer and deionized water. Finally, antibodies in 0.1 M pH 7.4 PBS buffer were added to the EDC/S-NHS activated QD solution. The final volume of the QD solution was less than 100 μL. The reaction incubated for 2 hours at RT on a shaker. After conjugation, Ab-QD conjugates were purified with PBS buffer by 50k Da centrifugal filter.

Appendix B: selection of optimal intravital imaging time with multiple molecular probes

Having optimized the i.v. injection of MMPs antibody conjugated QDs, we measured fluorescence signal from tumor of AOM/DSS mouse model at designated time points (Fig. 8) with anaesthetizing by inhaling isoflurane.

#207969 - $15.00 USD Received 14 Mar 2014; revised 19 Apr 2014; accepted 21 Apr 2014; published 29 Apr 2014

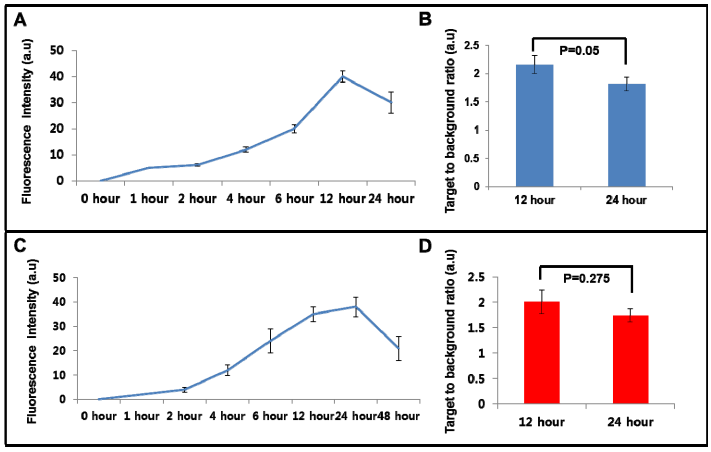

Fig. 8. The changes of fluorescence intensity from tumor over time with two different molecular probes. Change of fluorescence intensity by (A) MMP14 Ab-Yellow QD and (C) MMP9 Ab-Red QD probes over each time point. B and D: comparison of T/B ratios at 12 or 24 hour time points.

Until 12 hours after i.v. injection of MMP14 Ab-Yellow QD, the fluorescence intensity was increased. However, the signal became weak afterwards. Otherwise, the peak of fluorescence intensity was increased by 24 hours after i.v. injection of MMP9 Ab-Red QD and the signal became weak after 24 hours. Although the peak times appear different, each T/B ratio at 12 hours after injection of the probes was larger than at 24 hours. From these data we choose 12 hours after i.v. injection of our molecular probes as the optimal imaging time, and used this throughout our *in vivo* imaging experiments.

Acknowledgments

The authors thank the help from Miss. Ahra Cho for system scheme. The work is supported the Bio & Medical Technology Development Program and Basic Science Research Program through the National Research Foundation (NRF) funded by the Ministry of Science, ICT & Future Planning (No. 2011-0019633, 2011-0019632, 2012R1A1A1012853, and 2011-0030075) and by a grant from the Institute of Medical System Engineering.

#207969 - $15.00 USD Received 14 Mar 2014; revised 19 Apr 2014; accepted 21 Apr 2014; published 29 Apr 2014